ISSN 1674-1056
http://cpb.iphy.ac.cn
http://iopscience.iop.org/cpb
中国物理 B
Chinese Physics
中国物理 Chinese Physics B

Advanced characterization and calculation methods for rechargeable battery materials in multiple scales

Xin-Yan Li(李欣岩), Su-Ting Weng(翁素婷), Lin Gu(谷林)
Citation: Chin. Phys. B . 2020, 29(2): 028801 . **doi:** 10.1088/1674-1056/ab65ba
Journal homepage: http://cpb.iphy.ac.cn; http://iopscience.iop.org/cpb

What follows is a list of articles you may be interested in

Pair distribution function analysis: Fundamentals and application to battery materials

Xuelong Wang(王雪龙), Sha Tan(谭莎), Xiao-Qing Yang(杨晓青), Enyuan Hu(胡恩源)
Chin. Phys. B . 2020, 29(2): 028802 . **doi:** 10.1088/1674-1056/ab6656

High capacity sodium-rich layered oxide cathode for sodium-ion batteries

Gen-Cai Guo(郭根材), Changhao Wang(王长昊), Bang-Ming Ming(明帮铭), Si-Wei Luo(罗斯玮), Heng Su(苏恒), Bo-Ya Wang(王博亚), Ming Zhang(张铭), Hai-Jun Yu(尉海军), Ru-Zhi Wang(王如志)

Chin. Phys. B . 2018, 27(11): 118801 . **doi:** 10.1088/1674-1056/27/11/118801

Concentrated dual-salt electrolytes for improving the cycling stability of lithium metal anodes

Pin Liu(刘品), Qiang Ma(马强), Zheng Fang(方铮), Jie Ma(马洁), Yong-Sheng Hu(胡勇胜), Zhi-Bin Zhou(周志彬), Hong Li(李泓), Xue-Jie Huang(黄学杰), Li-Quan Chen(陈立泉)
Chin. Phys. B . 2016, 25(7): 078203 . **doi:** 10.1088/1674-1056/25/7/078203

All-solid-state lithium batteries with inorganic solid electrolytes: Review of fundamental science

Xiayin Yao(姚霞银), Bingxin Huang(黄冰心), Jingyun Yin(尹景云), Gang Peng(彭刚), Zhen Huang(黄祯), Chao Gao(高超), Deng Liu(刘登), Xiaoxiong Xu(许晓雄)
Chin. Phys. B . 2016, 25(1): 018802 . **doi:** 10.1088/1674-1056/25/1/018802

Scientific and technological challenges toward application of lithium-sulfur batteries

Ya-Xia Yin(殷雅侠), Hu-Rong Yao(姚胡蓉), Yu-Guo Guo(郭玉国)
Chin. Phys. B . 2016, 25(1): 018801 . **doi:** 10.1088/1674-1056/25/1/018801

TOPICAL REVIEW — Advanced calculation & characterization of energy storage materials & devices at multiple scale

Advanced characterization and calculation methods for rechargeable battery materials in multiple scales

Xin-Yan Li(李欣岩)[1,2], Su-Ting Weng(翁素婷)[1,2], and Lin Gu(谷林)[1,2,3,†]

[1] *Beijing National Laboratory for Condensed Matter Physics, Institute of Physics, Chinese Academy of Sciences, Beijing* 100190, *China*
[2] *School of Physical Sciences, University of Chinese Academy of Sciences, Beijing* 100049, *China*
[3] *Songshan Lake Materials Laboratory, Dongguan* 523808, *China*

(Received 1 November 2019; revised manuscript received 2 December 2019; accepted manuscript online 27 December 2019)

The structure–activity relationship of functional materials is an everlasting and desirable research question for material science researchers, where characterization and calculation tools are the keys to deciphering this intricate relationship. Here, we choose rechargeable battery materials as an example and introduce the most representative advanced characterization and calculation methods in four different scales: real space, energy, momentum space, and time. Current research methods to study battery material structure, energy level transition, dispersion relations of phonons and electrons, and time-resolved evolution are reviewed. From different views, various expression forms of structure and electronic structure are presented to understand the reaction processes and electrochemical mechanisms comprehensively in battery systems. According to the summary of the present battery research, the challenges and perspectives of advanced characterization and calculation techniques for the field of rechargeable batteries are further discussed.

Keywords: rechargeable batteries, advanced characterization and calculation, multiple scales

PACS: 88.80.ff, 82.45.Fk, 68.37.Ma, 61.50.Ah **DOI:** 10.1088/1674-1056/ab65ba

1. Introduction

Nowadays, rechargeable batteries have occupied most portable electronics and electric vehicle markets, including lithium-ion batteries (LIB), lead-acid batteries, and so on.[1–3] To achieve better electrochemical performance and sustainable ability of rechargeable batteries, sodium-ion batteries,[4,5] metal–air batteries,[6] and many other secondary batteries[7,8] have been studied for a long time. A great many advanced characterization and calculation tools are employed to reach an in-depth understanding of the structure–activity relationship of battery materials in order to design and build satisfactory batteries to meet the urgent requirements of better electronics energy storage systems.[9–11]

From different viewpoints in the present characterization and calculation research for rechargeable battery materials, four fundamental scales including real space, energy, momentum space, and time are discussed in depth in this review. The real space structure such as crystal structure, phase interfaces, and defects greatly influences the practical performance of batteries. The electronic structure in momentum space and various energy level transitions are both closely related to the thermal, electric, and mechanical properties, which are different directions to explore the origin of function in battery materials. For the scale of time, time-resolved structure and electronic structure evolutions are another concern for both the industrial community and the academic community. By reviewing recent studies, the future prospects of characterization and calculation methods in multiple scales are discussed.

2. Real space scale

To explore the structure–activity relationship of materials, the characterization and calculation of real space information are the most intuitive choice that comes to mind. According to the demands for information on different length scales, researchers have utilized many different techniques to analyze the materials at the macroscopic level, crystal lattice level, and atom level.

2.1. Macroscopic level

The performances of rechargeable batteries are significantly influenced by macroscopic structure, such as the morphology of electrodes, the particle size and shape, and the property of the solid electrolyte interface (SEI). It is the reason why a great many useful characterization and simulation tools have been used to extract the macroscopic information.

Scanning electron microscopy (SEM) has been one of the most popular tools in investigating the macroscopic morphology and topography of battery materials by means of collecting secondary electrons and backscattered electrons. Combining with a microbattery design, it is feasible to achieve real-time observation of the microbattery during discharge and charge, which is called *in situ* or *operando* SEM.[12,13] But

†Corresponding author. E-mail: l.gu@iphy.ac.cn

© 2020 Chinese Physical Society and IOP Publishing Ltd

SEM can only acquire surface and topography information. In contrast, transmission electron microscopy (TEM) collects the transmission electrons and can provide internal information of materials, for example, the thickness of the shell in a core–shell structure nanoparticle.[14,15] Other methods to image the macroscopic morphology such as transmission x-ray microscopy (TXM)[16,17] have not been used comprehensively. In other words, SEM and TEM have dominated the field of macroscopic real space detection of battery materials because of their high spatial resolution and convenience, and other techniques are still needed to be studied and optimized.

Macroscopic level simulations can help us to understand macroscopic in-depth phenomena in rechargeable batteries, such as stress, thermal stability, flow, multi-field coupling, and failure mechanism. So far, researchers have used phase-field models to study grain growth and roughening, crack evolution, the interaction of dislocations and solute, electromigration, multicomponent interdiffusion, etc. For example, Zuo *et al.* put forward a phase-field model coupling lithium diffusion, stress evolution, and crack propagation.[18] The model was applied to a silicon thin film electrode to explore the coupling effects on diffusion and crack propagation paths. Hu *et al.* developed a phase-field based multiscale model that enables generating nanoporous microstructures of different porosity and connectivity patterns based on the depth and energy of the surface (pore/electrolyte interface) to predict both the microstructure patterns and the effective properties of heterogeneous solid electrolytes.[19] Zhang *et al.* developed a nonlinear phase-field model for predicting Li dendrite growth at the electrode/electrolyte interface during the electrochemical deposition involving highly nonequilibrium processes. In the model, the Butler–Volmer type electrochemical kinetics was automatically reproduced at the moving diffusion interface and a revised Poisson–Nesters–Planck equation was further solved for ionic transport and local overpotential variation.[20]

When the scale of the phase-field model is larger than the micron scale or the free-boundary condition is to be dealt with, the finite element method is a better choice. The finite element method can help to understand some macroscopic engineering problems, such as the thermal stability and mechanical failure mechanism of batteries. The temperature distribution in the batteries has a significant impact on their safety and longevity. Guo *et al.* used a finite element method to develop a three-dimensional thermal abuse model on LIB (Fig. 1), which was coupled with electrochemical reactions and thermal responses to study in detail the temperature field distribution and evolution inside the cell.[21] Bower *et al.* described a finite element method for modeling deformation, diffusion, fracture, and electrochemical reactions in materials used as lithium-ion intercalation electrodes.[22] Vijayaraghavan *et al.* developed a finite element based neural search analytical model to analyze the crash for understanding the effect of various uncertainties in the LIB pack.[23] The intergranular and intragranular cracks in electrodes, SEI, and solid-state electrolyte are inevitable during the cycling of batteries and severely cause battery performance degradation. Today, many studies have focused on the cracking mechanism of battery materials.[24,25] Yan *et al.* analyzed the driving forces for crack propagation in $LiNi_{0.6}Mn_{0.2}Co_{0.2}O_2$ (NMC622) particles.[26] With the combination of inhomogeneous lithium distribution, phase transformation, crack surface pressure, and heat treatment, the coupling of thermal and mechanical effects can contribute to a high driving force for crack propagation and performance degradation of the NMC622 cathode. In conclusion, macroscale simulation is challenging and meaningful for solving practical problems in batteries.

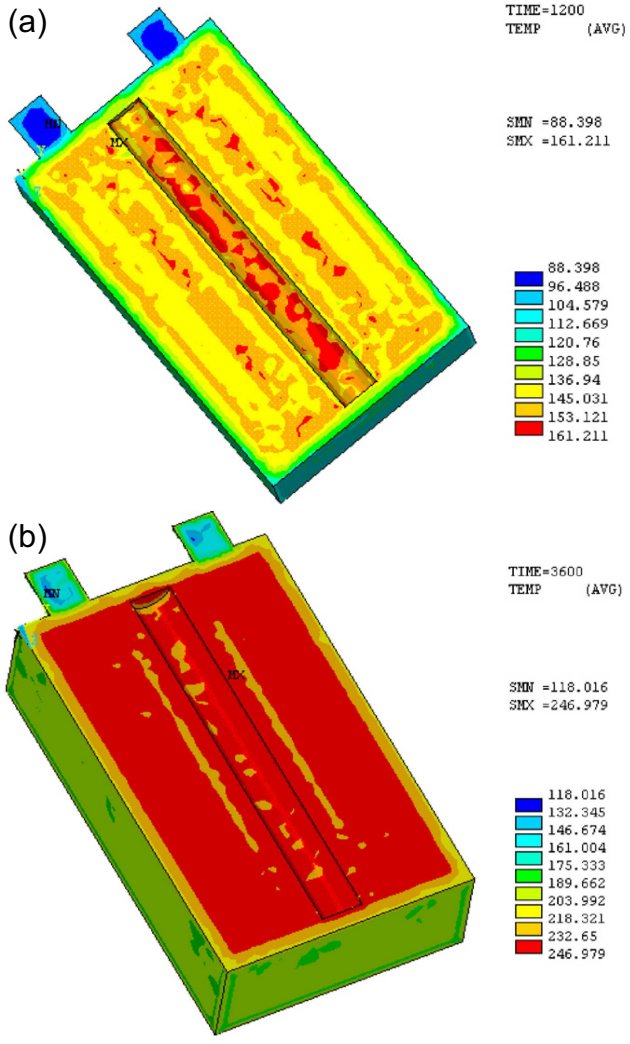


Fig. 1. Distribution of temperature at 155 °C using finite element modeling among different time scopes: (a) 1200 s, (b) 3600 s.[21]

2.2. Crystal lattice level

Most of the active materials in batteries are crystal or short-range ordered amorphous materials. The ability to probe and simulate the crystal structure is critical for linking the electrochemical performances and materials' structure. To date,

the diffraction techniques such as x-ray diffraction (XRD), neutron diffraction (ND), and electron diffraction are the most powerful tools to study the crystal lattice by a basic principle: incident microscopic particle interacts with crystal atoms, resulting in wave interference effect. Different crystal planes have different atomic arrangements, thus different planes have various diffraction directions. The relationship between different crystal plane and diffraction direction is given by the famous Bragg's law

$$2d\sin\theta = \lambda, \tag{1}$$

where d represents the interplanar spacing of the crystal plane, θ is the diffraction direction (incidence or reflection angle), and λ is the wavelength of the incident particle. By analyzing different diffraction direction combinations, various crystals can be distinguished precisely.

XRD utilizes x-rays (photons) as the incident particles. Collecting the data of θ and diffraction intensity and comparing them with standard substance information can provide the specific crystal structure and crystallinity of the sample. By Rietveld refinement, a great deal of useful information including lattice constant, atomic occupancy, and chemical stoichiometry of the material can be acquired to study the crystal structure and structure–activity relationship. It is worth mentioning that XRD provides the long-range average information because of the difficulty in converging the x-rays. On the other hand, *in situ* experiments are suitable for XRD. Synchrotron radiation source is able to offer higher intensity and photon flux than laboratory x-rays by several orders of magnitude. Combining synchrotron radiation source and *in situ* experiment techniques with XRD, real-time ultrafast data collection and deep penetration depth are satisfied with recent battery studies.[9]

Wu *et al.* demonstrated the crystal structure evolution of $Na_xCu_{0.27}Zn_{0.06}Mn_{0.67}O_2$ (NCZM) during the charge and discharge procedures of the sodium ion batteries by *in situ* synchrotron XRD.[27] In the region of $0.51 < x < 0.78$ of Fig. 2, the (002) peak position (2θ value) and intensity subtly decreased, which indicated a solid solution process. When the cathode was charged to 3.8 V that was the region of $0.42 < x < 0.51$, a significant peak position move and intensity change could be attributed to a phase transition reaction, which was verified by the result of electron energy-loss spectrum (EELS). The black arrow of the (002) peak suggested a highly disordered OP4 phase instead of the original P2 phase at 4.1 V, which demonstrated the stability of NCZM below 4.1 V.

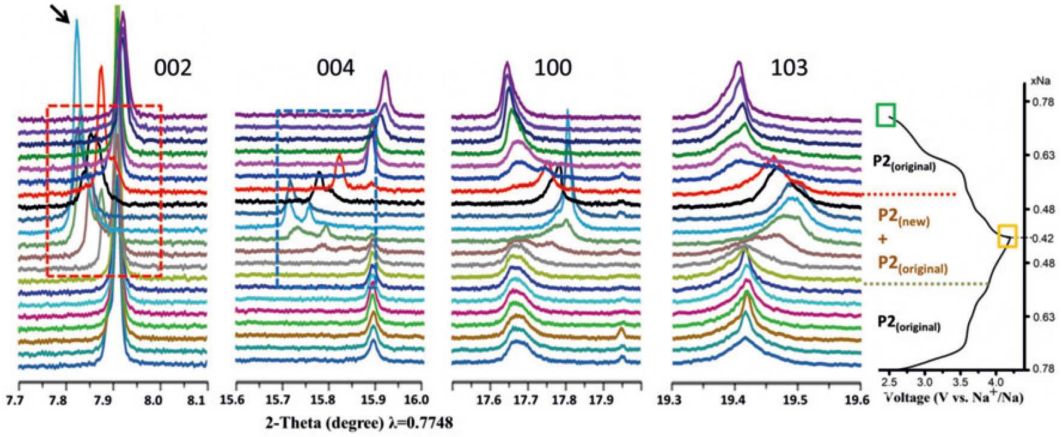


Fig. 2. Selected regions of *in situ* synchrotron XRD data and the sodium content–voltage curve.[27]

In contrast to x-rays, the scattering cross section of neutrons is irrelevant to atomic number Z, so it is better to distinguish light atoms and elements which have similar Z or isotopes than XRD. In addition, neutrons only interact with the atomic nucleus (different from x-rays that interact with electrons), resulting in a good penetration ability. However, there are some intrinsic limitations in ND. On the one hand, ND needs a large amount of materials. On the other hand, H atom strongly disturbs the analysis of the diffraction data. What is more, high-flux spallation neutron sources (SNS) which are urgently needed for ND technique are very scarce and the *in situ* experiments of ND are much more difficult than XRD.[9] To some extent, ND and XRD techniques complement each other in many different aspects.

Bruce's group investigated $Na_{2/3}Ni_{1/3-x}Mg_xMn_{2/3}O_2$ crystal lattice evolution with different substitution amount of Mg via ND and XRD.[28] Because of the different neutron scattering lengths of Mg and Mn, it is easy to characterize Mg^{2+}/Mn^{4+} ordering by ND. The comparison between XRD and ND data is shown in Fig. 3(a), in which ND shows more detail diffraction information. A series of ND diffraction data of $Na_{2/3}Ni_{1/3-x}Mg_xMn_{2/3}O_2$ is shown in Figs. 3(b) and 3(c). By combining with selected Rietveld refinement, they found that the crystallographic parameters are increasing with

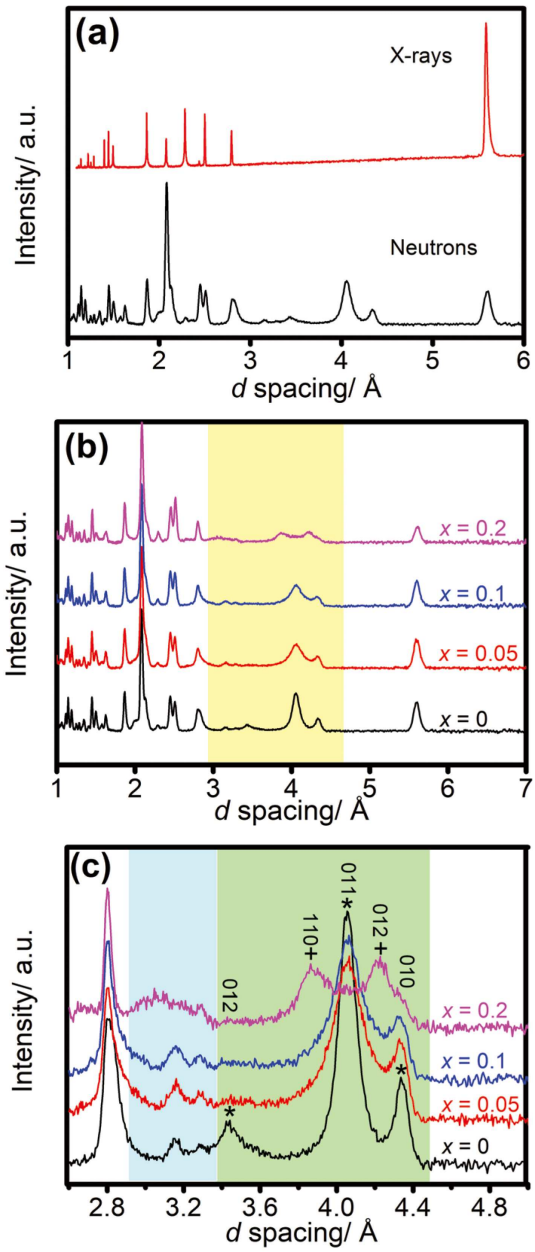


Fig. 3. (a) X-ray and neutron diffraction data comparison for $x = 0$. (b) Neutron diffraction data for $0 \leq x \leq 0.2$. (c) Zoomed-in yellow region of (b).[28]

the replacement of Mg^{2+} instead of Ni^{2+} because of the larger size of Mg^{2+}. In Fig. 3(c), the reflection at 4.1 Å implies the interplane Ni(Mg)/Mn long-range ordering by (011) crystal facet even at large magnesium content, which is different from a previous $Na_{2/3}Ni_{1/3}Mn_{2/3}O_2$ report.[29]

The principle of electron diffraction is similar to that of ND and XRD. Electron diffraction technique is always combined with TEM, thereby acquiring atomic and crystallographic information at the same time. The outstanding advantages of electron diffraction are the high intensity and the ability to analyze at nanoscale. However, the difficulties in quantitative analysis and the presence of the electron beam damage are still limiting this widely used diffraction technique. Nowadays, ultrafast electron diffraction (UED) technique equips with MeV electrons which differs from electron diffraction in TEM is used to study structural dynamics in many fields.[30–33] We will discuss more electron diffraction technique combing with TEM and electron energy loss spectrum (EELS) in the following section. In short, x-ray, neutron, and electron diffraction methods have their own respective advantages. Therefore, they are complementary techniques in detecting the crystal structure of battery materials to some extent.

In the field of simulation of crystal structure evolution, molecular dynamics and Monte Carlo simulations can both visually observe the migration of ions during electrochemical processes in the scale of crystal lattice level. Ma *et al.* created a dynamically adaptive approach in molecular dynamics simulations (Fig. 4) to reveal the molecular mechanisms and the reaction pathways in the conversion reaction of the FeF_2 electrode.[34] Intercalation along [001] rapid transport channels is accompanied by a slight reduction of charge density on multiple nearby Fe ions per Li ion until enough Li saturates a region, which causes the nearby Fe to lose sufficient charge and become destabilized, eventually forming Fe^0 nanocluster. The resultant nanostructures are fully consistent with the TEM observations. Methekar *et al.* used a kinetic Monte Carlo simulation to understand the passive SEI layer, the simulation results showed that the active surface coverage remains constant for the initial charging cycles and then decreases monotonically with the number of charging cycles.[35]

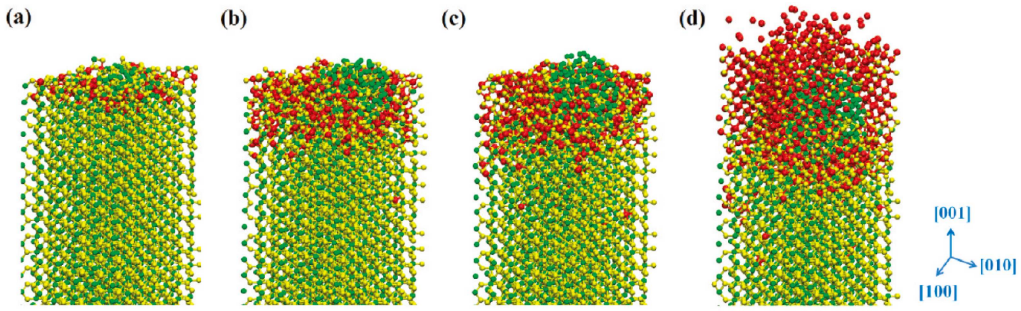


Fig. 4. Simulated reaction between Li and FeF_2 on the (001) surface of FeF_2. Fe–F bond is yellow, and Li–F bond is red. (a) System with 72 Li^+ already shows the growth of Fe metal cluster. (b) 288 Li^+ with a glassy Li–F region. (c) 360 Li^+, crystalline LiF is observed at the left corner. (d) 864 Li^+, crystalline LiF grows.[34]

2.3. Atom level

The atomic structure of defects and interfaces has a great influence on the performance of full batteries, so the capability to probe atomic information of materials is essential for the performance optimization of batteries. To date, many microscopic techniques have achieved sub-nanometer or even sub-angstrom resolution with different methods, such as scanning probe microscopy (SPM), high-resolution transmission electron microscopy (HRTEM), and scanning transmission electron microscopy (STEM).

SPM includes scanning tunneling microscopy (STM), atomic force microscopy (AFM), etc. which are based on quantum tunneling effect or atomic force and have atomic resolutions. STM[36,37] and AFM[38,39] have already been used to observe the atomic structure of battery materials for a long time and brought a novel view for surface information, especially for the phase interface. However, SPM is limited to the surface region. Hence, the bulk atomic information of electrodes and solid-state electrolytes cannot be acquired by SPM. That is where the electron microscopy is required.

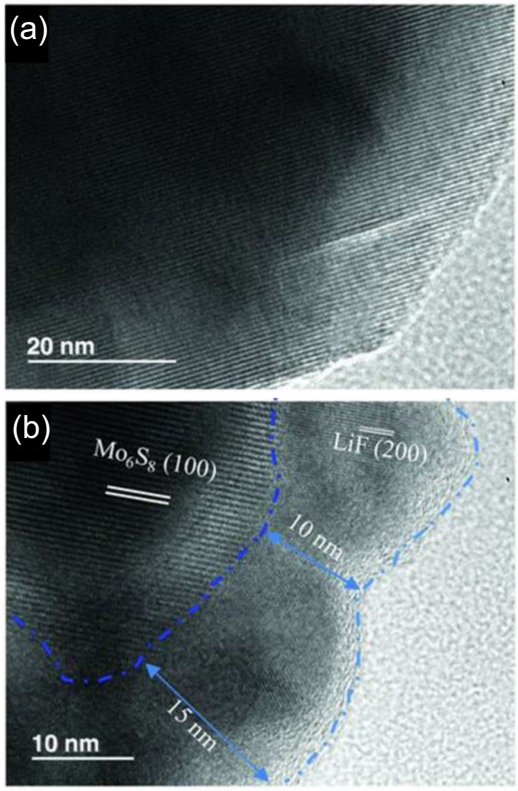


Fig. 5. HRTEM images of (a) pristine Mo_6S_8 and (b) cycled Mo_6S_8.[41]

HRTEM is an atomic scale technique with a long history and it has the ability to probe bulk information. In brief, it is an imaging mode of TEM and can directly image atomic columns by phase interference between diffracted beams and transmission beams.[40] To confirm the existence of SEI between the Mo_6S_8 anode and aqueous electrolyte, Suo *et al.* directly observed the SEI via HRTEM which is shown in Figs. 5(a) and 5(b).[41] $TFSI^-$ in the aqueous electrolyte is electrochemically reduced to LiF on the surface of Mo_6S_8 anode. The interplanar spacing of the LiF indicates its imperfect crystallinity. This crystalline $\sim$ 15 nm thick LiF-based SEI seems to differ from the composite interphase in nonaqueous electrolytes.[42]

Instead of utilizing the static incident electron beams of TEM, STEM scans the electron beams parallel to the optical axis and employs an annular detector to collect the scattered electrons.[40,43] Respectively, Pennycook *et al.* and Okunishi *et al.* proposed high angle annular dark field (HAADF)[44] and annular bright field (ABF)[45] imaging techniques in 1988 and 2009. The electron signal intensity in HAADF mode is almost proportional to $Z^{1.7}$ which is suitable for imaging relative heavy atoms[46,47] and in ABF mode is approximate $Z^{1/3}$ which is sensitive to light elements,[48] such as lithium and oxygen.

Gu's group constructed an all-solid-state nanobattery that consists of a $LiCoO_2$ cathode, Y and Ta doped LLZO solid-state electrolyte ($Li_{6.75}La_{2.84}Y_{0.16}Zr_{1.75}Ta_{0.25}O_{12}$), and a gold anode on a biasing nanochip by focus ion beam (FIB) milling.[49] The delithiation of the $LiCoO_2$ cathode was observed by HAADF and ABF after a high voltage biasing, which is an appropriate example for explaining the different features of HAADF and ABF. The pristine single crystal $LiCoO_2$ became nanosized polycrystal after delithiation and figure 6 shows its grain boundaries structure. Geographical phase analysis (GPA) was used for identifying the orientation of grains in Fig. 6(a), in which different colors indicate different orientations. Two types of boundaries were found that coherent twin boundaries are between different oriented grains and antiphase domain boundaries are between similarly oriented grains. The HAADF and ABF micrographs of coherent twin boundaries and antiphase domain boundaries are displayed respectively in Figs. 6(b)–6(e). It is obvious that only Co ion can be observed in the HAADF micrographs because of the weak signal of light elements. On the contrary, Li and O atoms can be distinguished clearly in the ABF micrographs, which is attributed to the $Z^{1/3}$ signal intensity relationship. Combining with theoretical calculations, the pathway of Li^+ along the boundaries is concluded for illuminating the lithium ion transportation mechanism in $LiCoO_2$ cathode.

STEM has a sub-angstrom resolution, which can directly reveal significant information on the physical and chemical properties of materials at the atomic level, such as phase transformation, surface/interface structure evolution, microscopic mechanisms of lithium ion diffusion and storage, and so on. Nevertheless, STEM still has some limitations. For example, the strong radiation of STEM can rapidly damage samples and both STEM and TEM images are actually two-dimensional

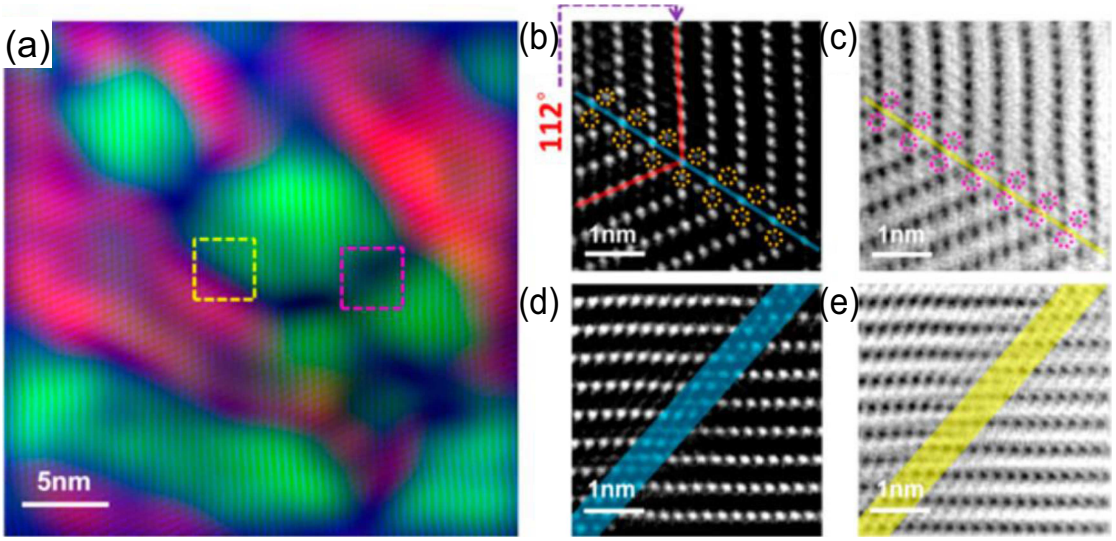


Fig. 6. (a) HAADF image of delithiated $LiCoO_2$ using the GPA method. (b) and (c) are HAADF and ABF images from the yellow region in (a), and (d) and (e) are HAADF and ABF images from the pink region in (a).[49]

projections of three-dimensional samples, which can be misleading. Therefore, the combination of computation and TEM imaging is very necessary, as the calculation can make up for the shortcomings of TEM imaging. The calculation methods are more applicable and not affected by the radiation damage, regardless of whether the sample is conductive or not. What is more, calculation methods can construct various periodic, even nonperiodic models, such as surface/interface models, which can provide a convenient interpretation of two-dimensional TEM images. Based on this, Yue *et al.* provided further insight on the intercalation/deintercalation process of Li and Na ions into $Fe_2(MoO_4)_3$ combining the first-principle thermodynamic calculations and direct atomic-scale observation by STEM.[50] With the combination of STEM and calculation, the "discrete occupation" and "pseudo-continuous" were proposed to describe the distinctly different occupation paths of Li and Na ions into $Fe_2(MoO_4)_3$.

3. Energy scale

Different from real space information, the energy state of an atom or a molecule can experience energy level transition when it undergoes external stimulation such as x-ray irradiation or electron impact. The energy level information is strongly correlated with electronic structure information of the sample which consists of charge, orbital, and even spin information of the elements. In terms of different external stimulation methods, researchers have developed x-ray energy-dispersive spectroscopy (XEDS), EELS, which are generated from the interaction of electrons and sample, x-ray absorption spectroscopy (XAS), x-ray photoelectron spectroscopy (XPS), which rely on the x-ray sources.

XEDS is a widespread option for SEM and TEM at present and it is easy to use for distinguishing various elements. In an electron microscope, a high-energy electron beam penetrates outer-shell electron cloud and interacts with inner-shell electrons so that the inner-shell electrons are ejected. Subsequently, the outer-shell electrons fill the empty energy level and emit characteristic x-rays. If the incident electrons penetrate through the electron shells and directly interact with nuclei, the electrons will decelerate and emit continuous x-rays that are called bremsstrahlung x-rays which need to be filtered in the spectroscopy analysis.[51] In short, XEDS collects the signal of x-rays while differentiates diverse elements by characteristic x-rays. The application of XEDS mapping has become a feasible and effective way to discover elements' distribution in real space for energy materials.[52,53]

In TEM, EELS collects transmission electrons and analyzes their energy distribution. Inelastic transmission electrons also contain electronic structure information inside the loss of energy. Comparing with XEDS, EELS can detect and quantify all the elements, meanwhile offers atomic level spatial resolution and valence state level energy resolution. Gong *et al.* studied the delithiation of $LiNi_{0.5}Mn_{1.5}O_4$ cathode from various zone axes in atomic scale.[54] HAADF image of antiphase boundaries from ⟨112⟩ zone axe is shown in Fig. 7(a) and the EELS line scan trajectory is in direction of the blue arrow. Figures 7(b)–7(d) show the EELS spectra of O, Mn, and Ni along the line scan direction. It is easy to find that the *L*-edge of Mn shifts to left and the *L*-edge of Ni shifts to right, which manifest the reduction of Mn and the oxidation of Ni. The intensity periodic change suggests great content change at the antiphase boundaries and figure 7(e) is the distance–intensity relationship. The loss of O and Mn and the accumulation of Ni at the antiphase boundaries may attribute to the reconstruction phenomenon in the boundaries. A similar result is shown in Figs. 7(f)–7(j) except for no clear change in oxygen content in the region of migration-front.

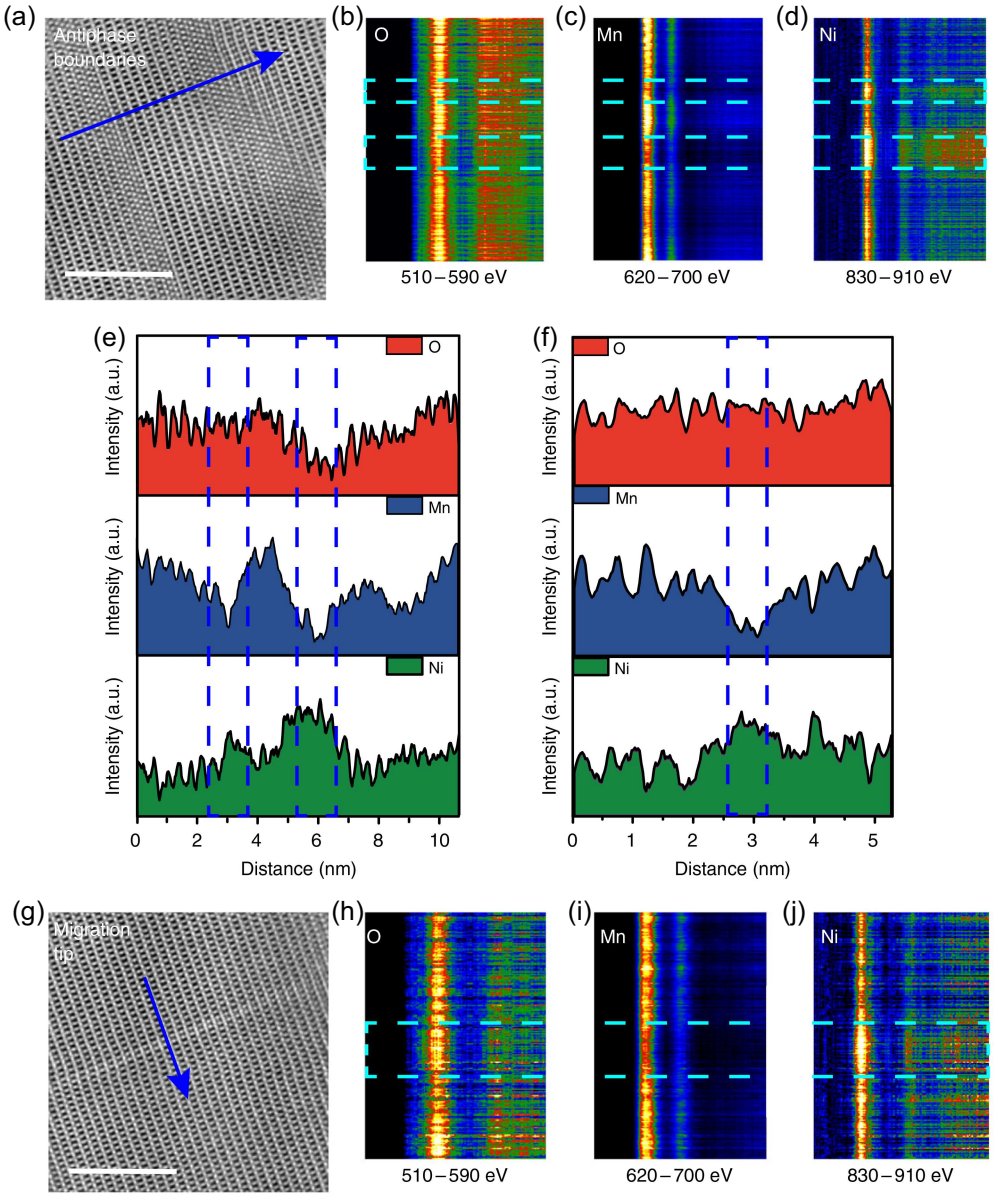


Fig. 7. (a) HAADF image of antiphase boundaries with blue arrow showing the EELS line scan trajectory. (b)–(d) EELS spectra of O, Mn, and Ni. The dashed rectangle represents two antiphase boundaries in (a). Elements content distribution results of EELS from antiphase boundaries region (e) and migration front region (f). (g) HAADF image of migration front area with blue arrow showing the EELS line scan trajectory. (h)–(j) EELS spectra of O, Mn, and Ni. The dashed rectangle represents migration front in (g). Scale bar, 5 nm.[54]

With tuning the photon energy to excited electron energy, XAS can obtain electronic structure by energy level transition. A typical x-ray absorption spectrum comprises x-ray absorption near-edge structure (XANES) and extended x-ray absorption fine structure (EXAFS). XANES is sensitive to valence state and coordination of elements and EXAFS is good for quantifying local structural information.[4] Su's group traced the valence state of Fe in spinel Fe_3O_4 cathode to investigate the cause of capacity fading via synchrotron XAS.[55] XANES of Fe *K*-edge of different cycled Fe_3O_4 cathode is shown in Fig. 8(a). Fe *K*-edge becomes increasingly similar between discharge and charge states as the cycle goes on, which means the redox reaction is limited after long cycles. Figure 8(b) is the content of Fe^0, Fe^{2+}, and Fe^{3+} by fitting XANES data with a linear combination of reference Fe^0, Fe^{2+}, and Fe^{3+} and figures 8(c)–8(e) present the proportion evolution of these three valence states. During the discharge process, both intercalation ($Fe^{3+} \rightarrow Fe^{2+}$) and conversion reactions (Fe^{3+}, $Fe^{2+} \rightarrow Fe^0$) are found, but some of Fe elements are not reduced to metallic Fe. With the increase of the cycle times, the proportion of metallic Fe continuously enhances. It suggests a passivated redox reaction after 100 cycles and this phenomenon contributes to the capacity fading of the conversion cathode. At present, XAS and EELS are the most powerful and reliable characterization methods to detect the energy level transition, especially for the valence transition of transition elements in electrode materials.

In the domain of surface analysis, XPS exploits core-level photoemission to probe the valence state and the element composition of samples. Although the sensitivity of XPS

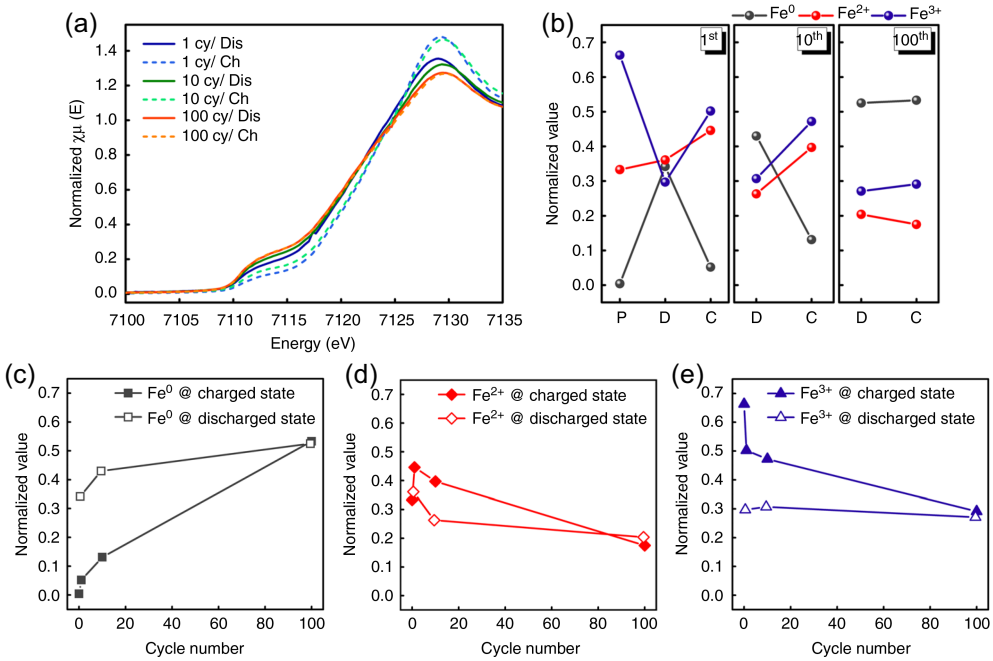


Fig. 8. (a) XANES spectra of electrode materials at discharge and charge states of different cycles. (b) Quantification of the oxidation states of Fe for different cycles. Pristine, discharged, and charged are represented with P, D, and C, respectively. (c)–(e) Quantification of the oxidation states of Fe as a function of cycle number.[55]

is no match for XAS, the direct relationship between photoelectron and energy level makes XPS a great technique in extracting chemical information from sharp core-level peaks from the same elements.[56] Nowadays, a great many interfaces and protected layers studies have employed XPS for *in situ* or *ex situ* observing the surface information of various batteries.[57,58]

Compared to characterization tools, the energy scale calculations can predict the stability, defect formation energy, and ion transport mechanism of electrode materials. The stability of cathode material is very important for LIB, as cathode material is still the lithium source of the battery currently. If the cathode is not stable in the electrochemical reaction processes, the side reactions will lead to the rapid decay of battery performance, and even bring safety risks. Wang *et al.* presented a new method based on the first-principles approach for predicting the thermodynamics of thermal degradation of charged cathode materials for LIB.[59] The calculated decomposition heat for three systems is in good agreement with experiments on three cathode materials: Li_xNiO_2, Li_xCoO_2, and $Li_xMn_2O_4$. Gao *et al.* used first-principles calculations within the Perdew–Burke–Ernzerhof exchange–correlation functional and the Hubbard-type correction U (PBE $+U$) scheme to show that Mo doping is beneficial for improving both the dynamic and thermodynamic properties of Li_2MnO_3.[60] Figure 9 shows the reaction enthalpy and Gibbs free energy in the oxygen release process of different delithiated Li_yMnO_3 and $Li_yMn_{0.75}Mo_{0.25}O_3$ calculated by PBE $+U$ exchange correlation potential, and the structural stability of Li_2MnO_3 doped with Mo is greatly improved compared with the undoped Li_2MnO_3.

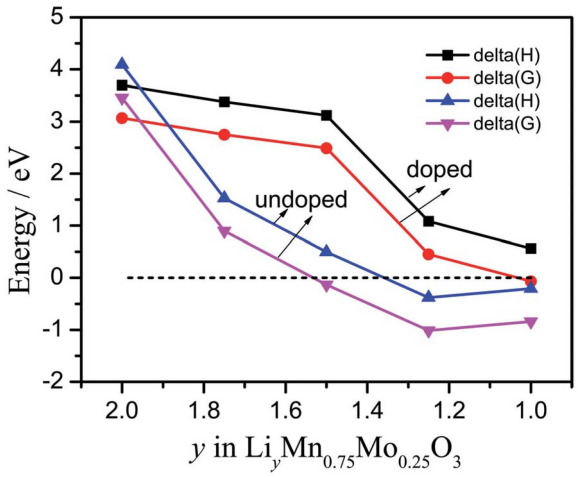


Fig. 9. Calculated reaction enthalpy and Gibbs free energy for O_2 release from different delithiation states Li_yMnO_3 and $Li_yMn_{0.75}Mo_{0.25}O_3$, where $y = 2$, 1.75, 1.5, 1.25, and 1, for Li_2MnO_3 and $Li_2Mn_{0.75}Mo_{0.25}O_3$, respectively.[60]

Defects and impurities in materials can also change many properties of materials, including the electronic conductance and ionic conductance. Hoang *et al.*[61] reported a first-principles study of various monovalent elements doped into different lattice positions of $LiFePO_4$.[61] They found that it is possible to effectively enhance the electronic conductivity of $LiFePO_4$ through defect control. The path and energy barrier of Li^+ transportation are directly related to the rate performance and polarization of batteries. Ouyang *et al.* used

the adiabatic trajectory method to obtain the migration energy barriers for the migration of Li ions and Cr ions along the one-dimensional diffusion pathway in pure and Cr doped $LiFePO_4$ from first-principles calculations.[62] The results showed that while Li ions can diffuse along the diffusion pathway easily, Cr ions do not easily diffuse away from their initial positions. This means that the heavy Cr ions will block the one-dimensional diffusion pathway of the material. Yang *et al.* investigated the mechanisms for thermal self-diffusion of Li ions in fully lithiated $LiFePO_4$ with spin polarized *ab initio* molecular dynamics calculations.[63] It was found that Li ion diffusion is not a continuous process but through a series of jumps from one site to another.

4. Momentum space scale

The physical quantities that depend on momentum space such as lattice vibration and energy band determine the thermal, mechanical, electrical, and many other properties of materials. However, the methods of momentum characterization in the field of rechargeable batteries still scarcely attach importance to the dispersion in momentum space because of the complexity of the battery system. In this section, we will focus on phonon dispersion and energy band structure of battery-related materials.

4.1. Phonon dispersion

The energy of a phonon mode is on the order of 10–10^2 meV, therefore an energy transfer around vibration energy must be achieved to characterize the vibrational modes of materials. At present, many different techniques have successfully probed the phonon dispersion. Inelastic scattering techniques including inelastic x-ray scattering[64,65] and inelastic neutron scattering[66,67] are old-style methods, but they are rarely used in battery research. Optical spectroscopy exploits the inelastic scattering of photons to detect the vibrational modes, for example, Raman spectroscopy, which has been widely applied for detecting the structural variations of battery materials.[68] Zaghib *et al.* used *in situ* Raman spectroscopy to investigate the vibrational modes in Cr/Co-doped $LiMn_{1.5}Ni_{0.5}O_4$ cathode and study the valence state change of Ni and Mn in real time.[69]

Two-dimension materials are of great importance in the field of rechargeable batteries. Recently, Kazu *et al.* reported a novel method to simultaneously map the vibration in graphene nanostructures in real space and momentum space.[70] Different from low-spatial-resolution inelastic x-ray (neutron) scattering techniques and low-momentum-transfer optical spectroscopy, EELS in transmission can provide local vibrational modes of two-dimension monolayer materials for several Brillouin zones at the nanometer scale. There must be a tradeoff between spatial resolution and momentum resolution because of the uncertainty principle. With the energy resolution of 30 meV full width at half maximum (FWHM), the momentum resolution of ± 0.1–0.2 Å^{-1}, and the probe size of 10–40 nm, phonon dispersions along different momentum space directions are measured and they are perfectly accord with simulated results. Except for the missing of the low-energy region, details of the phonon dispersions are mostly described.

Yao *et al.* used first-principles density functional theory (DFT) calculations to investigate both the disordered rock salt-type $Li_4Mn_2O_5$ structure and the ordered ground-state structure.[71] From Fig. 10(a), the energy of $Li_4Mn_2O_5$ is slightly higher than that of Li_2O and $LiMnO_2$, so $Li_4Mn_2O_5$ is not stable at 0 K. Their DFT-calculated phonon dispersion of the *Cmmm* $Li_4Mn_2O_5$ is provided in Fig. 10(b), and no imaginary phonons are shown, which indicates that $Li_4Mn_2O_5$ is dynamically stable. By computing the harmonic phonons and vibrational entropies of $Li_4Mn_2O_5$, $LiMnO_2$, and Li_2O, the relationship between free energy and temperature has been revealed, as shown in Fig. 10(c).

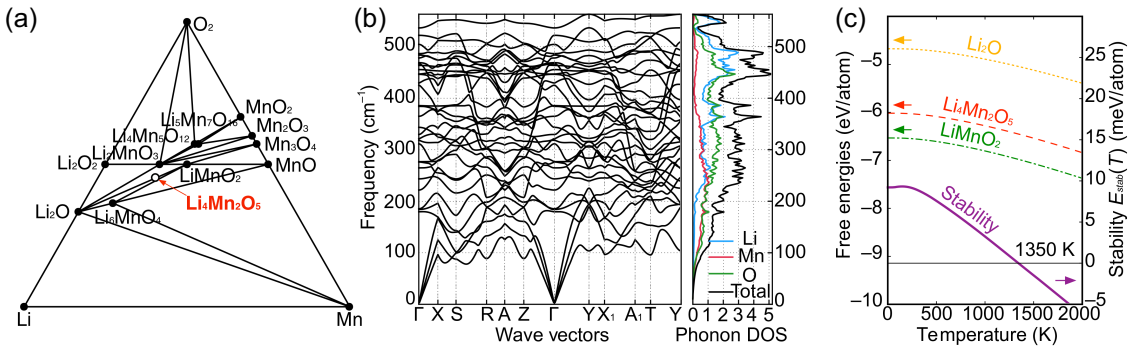


Fig. 10. Thermodynamic and dynamic stabilities of $Li_4Mn_2O_5$. (a) Calculated Li–Mn–O ($T = 0$ K) phase diagram. The $Li_4Mn_2O_5$ phase is slightly higher in energy (13.6 meV per atom) relative to the ground-state phase: a mixture of Li_2O and $LiMnO_2$. (b) Phonon dispersion of the ground-state $Li_4Mn_2O_5$ and (c) calculated temperature-dependent free energy of $Li_4Mn_2O_5$ (red dashed line), Li_2O (orange dotted line), and $LiMnO_2$ (green dotted line), as well as the stability (purple solid line) of $Li_4Mn_2O_5$ versus temperature relative to Li_2O and $LiMnO_2$ phase mixtures. $Li_4Mn_2O_5$ is dynamically stable and can be entropically stabilized at $\sim$ 1350 K.[71]

4.2. Energy band

The electronic energy band of solid materials is very important for battery design, for it describes the quantum-mechanic-allowable electron energy state which strongly influences the electrical property of electrodes and solid-state electrolytes. The electronic structure of the battery material is closely related to their electrochemical properties, for example, the chemical stability of the interface between the electrode and the electrolyte can be derived from the density of energy states,[72] the rate performance is related to the electronic conductivity of the electrodes,[73] solid electrolyte materials require electronic insulation properties, which are related to the width of the energy gap.[74]

Nevertheless, experimental characterization of the energy band is still limited to a few techniques such as angle-resolved photoemission spectroscopy (ARPES) and resonance Raman spectroscopy (RRS). ARPES directly observes the distribution of electrons in momentum space by photoemission electrons and it has become one of the most indispensable techniques for characterizing the physical property.[75] Usachov *et al.* employed ARPES to study the energy band of N-doped graphene.[76] The nitrogen impurities could tune the band structure and carrier concentration of N-doped graphene for optimizing the performance of energy devices.

If the energy of the incoming or outgoing photon matches the electronic transition energy of the sample, the Raman cross section will notably increase, which is called RRS.[77,78] As a result, RRS relates the Raman signals to the electronic energy band. Today, the energy band structure of many types of materials has been studied by RRS.[79,80] These kinds of momentum-related characterizations in the momentum space enlighten the followers to discover the quality of battery materials from a brand-new angle.

The calculation of energy band is scarce in the field of rechargeable batteries none the less. Chen *et al.* demonstrated that carbon foams (CFs) exhibit good stabilities and pore-size dependent electronic properties, which are related to the size-dependent band gaps of graphene nanoribbons (GNRs) through first-principles calculations.[81] Then they used 48Z_S_I as an example to calculate the band structures of monolayer graphene nanoribbons-based asymmetric zigzag CFs to find out the rules (Fig. 11). Based on this, they found that: when l, m, and n all equal to $3n$ or $3n+2$, if at least one is equal to $3n$, the CF is a wide-band-gap semiconductor, otherwise, it is a narrow-band-gap semiconductor. When only one of the three widths is equal to $3n+1$, the CF has a small E_g, if more than one, it is metallic. However, researchers seem to pay more attention to the density of states (DOS) of electrons. Seo *et al.* used *ab initio* calculations to demonstrate which specific chemical and structural features lead to electrochemically active oxygen states in cathode materials by calculating the projected DOS (pDOS) of the oxygen 2p states of the three oxygen environments.[82]

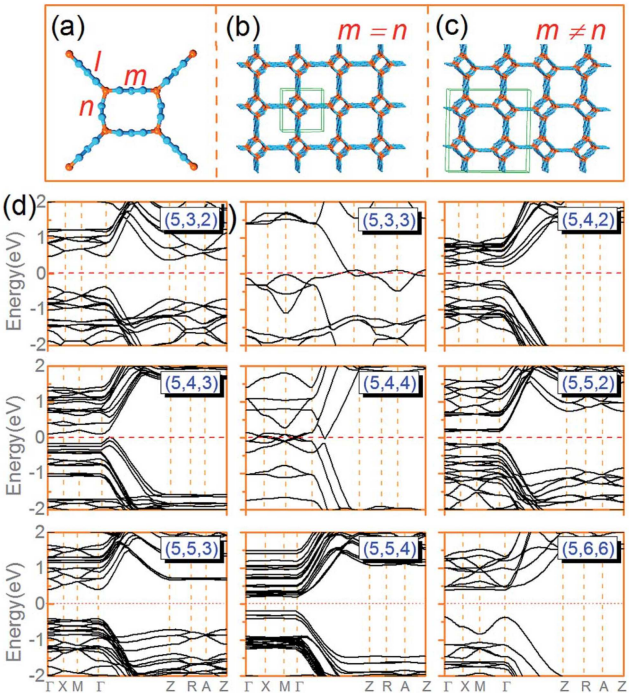


Fig. 11. The schematics of asymmetric 48Z_$S_I(l,m,n)$ networks and the corresponding band structures. (a) Three-wing GNRs building block of asymmetric CFs and three width degrees of freedom, l, m, n, are considered. (b) and (c) $m=n$ and $m\neq n$ asymmetric CFs, respectively. The orange and cyan sticks indicate the sp^3 and sp^2 C atoms, respectively. (d) The band structures of (5, 3, 2), (5, 3, 3), (5, 4, 2), (5, 4, 3), (5, 4, 4), (5, 5, 2), (5, 5, 3), (5, 5, 4), and (5, 6, 6).[81]

5. Time scale

On account of the demand for higher time resolution, especially for ultrafast charge and discharge of batteries and *in situ* experiments, the time-resolved characterization tools are critical for ultrafast dynamic processes. Unlike picosecond in the field of solar cell,[83] the time-resolved characterizations always focus on the magnitude of second referring to rechargeable batteries, such as time-resolved XRD, XAS, and *in situ* TEM, because of the sluggish dynamic reaction in electrode and electrolyte scale. However, the dynamics of atomic scale processes in millisecond and even picosecond scale are rarely studied at present.

In situ TEM directly observes the real-time evolution of electrode that is feasible to acquire the mechanism of reactions in batteries. The first research of lithiation evolution by Huang *et al.* reached a time resolution of a half second for the morphology evolution of the SnO_2 anode in 2010.[84] Lately, He *et al.* studied the lithiation of $SnSe_2$ by *in situ* HRTEM with a similar time resolution but a higher spatial resolution to clearly observe the lattice fringes of $SnSe_2$.[85] It is obvious that a tradeoff restricts the spatial resolution and the time resolution. Atomic spatial resolution and better time resolution are still needed to achieve for studying the microscopic

mechanism of the battery system. The x-rays related tools also demand higher time resolution for detecting the processes of the crystal structure evolution and valence state evolution.[86] Yang *et al.* used *in situ* XRD and XAS to characterize the structural and valent changes of $LiNi_{1/3}Mn_{1/3}Co_{1/3}O_2$ cathode at different charge rates.[87] The time resolution of XRD and XAS is also on the order of several seconds. In general, the time resolution of characterization tools in the research of batteries is around several seconds nowadays and it is enough for observing the macroscopic phenomenon. But for microscopic behaviors, a higher time resolution is still required for investigating in-depth mechanism of the battery system.

As for the computation, Leung *et al.* used *ab initio* molecular dynamics (AIMD) simulations to study ethylene carbonate (EC) decomposition process in the electron-rich anode regions in real-time. With an explicit treatment of the EC liquid environment, an excess electron can induce EC decomposition within AIMD timescales. Both C_E–O_1 and C_C–O_1 cleavages occur, yielding CO_3^{2-} and $OC_2H_4O^{2-}$, respectively.[88] $OC_2H_4O^{2-}$, or HOC_2H_4OH if a proton source exists, potentially reacts with CO_2 or CO_3^{2-} at longer time scales to form $(CH_2CO_3Li)_2$, a main SEI component.

6. Conclusion and perspective

Advanced characterization and calculation methods provide an opportunity to investigate the structure–activity relationship of rechargeable battery materials comprehensively. From four different scales, the structure and electronic structure can be generally described. In this review, we have introduced the most representative characterization and calculation tools that have been used in battery systems from the scales of real space, energy, momentum space, and time. Overall, present studies in the field of rechargeable batteries focus on the information of real space structure and energy level transition processes, nevertheless, it is scarce to study the material properties in momentum space and ultrafast time scale (namely, millisecond or less). In addition, the combined analysis of different scales is useful but scarcely reported for battery studies. Therefore, some potential directions for future development of characterization and calculation methods are discussed below.

Analysis combining multiple scales is the first direct choice to achieve a multi-dimension assessment of battery material properties. For example, simultaneous analysis of STEM image and EELS, even employing the time-resolved TEM technique, can draw a picture including the real space, energy level transition, and ultrafast dynamic information, which is able to boost the investigation of battery reaction mechanisms. Besides, the development of *in situ* or *operando* techniques has brought a direct time-resolved method to observe the dynamic evolution of energy materials, especially for high-rate discharge/charge processes. However, the time resolution of the present *in situ* technique is mostly confined to sub-second scope in the field of rechargeable batteries. Better time resolution such as sub-millisecond is badly needed to detect the phase transition or some other rapid processes in the nonequilibrium system of reacting batteries and further improved computing power can simulate more complicated and rapid processes. Learning from some up-to-date research,[89] machine learning is suited for us to find some significant materials rather than repetitive work which wastes a large amount of time. Finally, pretty few reports about momentum dispersion of phonons or electrons are published, which probably suggests that the energy band structure and vibration modes of materials are still not rigorously studied in the field of rechargeable batteries.

To date, the characterization and calculation methods for rechargeable batteries are extensive developed, but problems of each method still limit the applications, such as limited resolution and poor computational efficiency. However, with the combination of multiple scales analysis, a fairly good description of material structure and electronic structure could be realized for investigating the structure–activity relationship of energy materials or other functional materials and designing desirable materials with better performance.

References

[1] Kim T, Song W, Son D Y, Ono L K and Qi Y 2019 *J. Mater. Chem. A* **7** 2942
[2] Winter M, Barnett B and Xu K 2018 *Chem. Rev.* **118** 11433
[3] Armand M and Tarascon J M 2008 *Nature* **451** 652
[4] Shadike Z, Zhao E, Zhou Y N, Yu X, Yang Y, Hu E, Bak S, Gu L and Yang X Q 2018 *Adv. Energy Mater.* **8** 1702588
[5] Grey C P and Tarascon J M 2017 *Nat. Mater* **16** 45
[6] Xiang J, Yang L, Yuan L, Yuan K, Zhang Y, Huang Y, Lin J, Pan F and Huang Y 2019 *Joule* **3** 2334
[7] Wu Y, Huang H B, Feng Y, Wu Z S and Yu Y 2019 *Adv. Mater.* **31** e1901414
[8] Manthiram A, Fu Y, Chung S H, Zu C and Su Y S 2014 *Chem. Rev.* **114** 11751
[9] Zhu H, Huang Y, Zhu H, Wang L, Lan S, Xia X and Liu Q 2019 *Small Methods* 1900223
[10] Liu D, Shadike Z, Lin R, Qian K, Li H, Li K, Wang S, Yu Q, Liu M, Ganapathy S, Qin X, Yang Q H, Wagemaker M, Kang F, Yang X Q and Li B 2019 *Adv. Mater.* **31** 1806620
[11] Lu J, Wu T and Amine K 2017 *Nat. Energy* **2** 17011
[12] Golozar M, Hovington P, Paolella A, Bessette S, Lagace M, Bouchard P, Demers H, Gauvin R and Zaghib K 2018 *Nano Lett.* **18** 7583
[13] Zheng H, Xiao D, Li X, Liu Y, Wu Y, Wang J, Jiang K, Chen C, Gu L, Wei X, Hu Y S, Chen Q and Li H 2014 *Nano Lett.* **14** 4245
[14] Zhang J, Zhang M, Qiu L, Zeng Y, Chen J, Zhu C, Yu Y and Zhu Z 2019 *J. Mater. Chem. A* **7** 19045
[15] Liu Y, Kou W, Li X, Huang C, Shui R and He G 2019 *Small* **15** e1902431
[16] Landa Medrano I, Sorrentino A, Stievano L, Ruiz de Larramendi I, Pereiro E, Lezama L, Rojo T and Tonti D 2017 *Nano Energy* **37** 224
[17] Pereiro E, Nicolas J, Ferrer S and Howells M R 2009 *J. Synchrotron Radiat* **16** 505
[18] Zuo P and Zhao Y P 2015 *Phys. Chem. Chem. Phys.* **17** 287

[19] Hu J M, Wang B, Ji Y, Yang T, Cheng X, Wang Y and Chen L Q 2017 *ACS Appl. Mater Interfaces* **9** 33341
[20] Zhang H W, Liu Z, Liang L, Chen L, Qi Y, Harris S J, Lu P and Chen L Q 2014 *ECS Transactions* **61** 1
[21] Guo G, Long B, Cheng B, Zhou S, Xu P and Cao B 2010 *J. Power Sources* **195** 2393
[22] Bower A F and Guduru P 2012 *Modell. Simul. Mater. Sci. Eng.* **20** 045004
[23] Vijayaraghavan V, Shui L, Garg A, Peng X and Singh V P 2019 *Eng. Comput.* **35** 115
[24] Xu R and Zhao K 2018 *J. Mech. Phys. Solids* **121** 258
[25] Zhang S, Zhao K, Zhu T and Li J 2017 *Prog. Mater. Sci.* **89** 479
[26] Yan P, Zheng J, Chen T, Luo L, Jiang Y, Wang K, Sui M, Zhang J G, Zhang S and Wang C 2018 *Nat. Commun.* **9** 2437
[27] Yan Z C, Tang L, Huang Y Y, Hua W B, Wang Y, Liu R, Gu Q F, Indris S, Chou S L, Huang Y H, Wu M H and Dou S X 2019 *Angew. Chem. Int. Edit.* **58** 1412
[28] Tapia R N, Dose W M, Sharma N, Chen H, Heath J, Somerville J W, Maitra U, Islam M S and Bruce P G 2018 *Energy & Environ. Sci.* **11** 1470
[29] Paulsen J M, Donaberger R A and Dahn J R 2000 *Chem. Mater.* **12** 2257
[30] Yang J, Zhu X, Wolf T J A, Li Z, Nunes J P F, Coffee R, Cryan J P, Gühr M, Hegazy K, Heinz T F, Jobe K, Li R, Shen X, Veccione T, Weathersby S, Wilkin K J, Yoneda C, Zheng Q, Martinez T J, Centurion M and Wang X 2018 *Science* **361** 64
[31] Mo M Z, Chen Z, Li R K, Dunning M, Witte B B L, Baldwin J K, Fletcher L B, Kim J B, Ng A, Redmer R, Reid A H, Shekhar P, Shen X Z, Shen M, Sokolowski Tinten K, Tsui Y Y, Wang Y Q, Zheng Q, Wang X J and Glenzer S H 2018 *Science* **360** 1451
[32] Yang J, Guehr M, Vecchione T, Robinson M S, Li R, Hartmann N, Shen X, Coffee R, Corbett J, Fry A, Gaffney K, Gorkhover T, Hast C, Jobe K, Makasyuk I, Reid A, Robinson J, Vetter S, Wang F, Weathersby S, Yoneda C, Centurion M and Wang X 2016 *Nat. Commun.* **7** 11232
[33] Weathersby S P, Brown G, Centurion M, Chase T F, Coffee R, Corbett J, Eichner J P, Frisch J C, Fry A R, Guhr M, Hartmann N, Hast C, Hettel R, Jobe R K, Jongewaard E N, Lewandowski J R, Li R K, Lindenberg A M, Makasyuk I, May J E, McCormick D, Nguyen M N, Reid A H, Shen X, Sokolowski Tinten K, Vecchione T, Vetter S L, Wu J, Yang J, Durr H A and Wang X J 2015 *Rev. Sci. Instrum.* **86** 073702
[34] Ma Y and Garofalini S H 2012 *J. Am. Chem. Soc.* **134** 8205
[35] Methekar R N, Northrop P W C, Chen K, Braatz R D and Subramanian V R 2011 *J. Electrochem. Soc.* **158** A363
[36] Ren J, Wang Y, Zhao J, Tan S and Petek H 2019 *J. Am. Chem. Soc.* **141** 4438
[37] Seidl L, Bucher N, Chu E, Hartung S, Martens S, Schneider O and Stimming U 2017 *Energy & Environ. Sci.* **10** 1631
[38] Wan J, Hao Y, Shi Y, Song Y X, Yan H J, Zheng J, Wen R and Wan L J 2019 *Nat. Commun.* **10** 3265
[39] Chen X, Lai J, Shen Y, Chen Q and Chen L 2018 *Adv. Mater.* **30** 1802490
[40] Liu X and Gu L 2018 *Small Methods* **2** 1800006
[41] Suo L, Borodin O, Gao T, Olguin M, Ho J, Fan X, Luo C, Wang C and Xu K 2015 *Science* **350** 938
[42] Xu K 2014 *Chem. Rev.* **114** 11503
[43] Tong Y X, Zhang Q H and Gu L 2018 *Chin. Phys. B* **27** 066107
[44] Pennycook S J and Boatner L A 1988 *Nature* **336** 565
[45] Okunishi E, Ishikawa I, Sawada H, Hosokawa F, Hori M and Kondo Y 2009 *Microsc. Microanalysis* **15** 164
[46] Loane R F, Kirkland E J and Silcox J 1988 *Acta Crystallogr. Sect. A* **44** 912
[47] Kirkland E J, Loane R F and Silcox J 1987 *Ultramicroscopy* **23** 77
[48] Findlay S D, Shibata N, Sawada H, Okunishi E, Kondo Y and Ikuhara Y 2010 *Ultramicroscopy* **110** 903
[49] Gong Y, Zhang J N, Jiang L, Shi J A, Zhang Q, Yang Z, Zou D, Wang J, Yu X, Xiao R, Hu Y S, Gu L, Li H and Chen L 2017 *J. Am. Chem. Soc.* **139** 4274
[50] Yue J L, Zhou Y N, Shi S Q, Shadike Z, Huang X Q, Luo J, Yang Z Z, Li H, Gu L, Yang X Q and Fu Z W 2015 *Sci. Rep.* **5** 8810
[51] Williams D B and Carter C B 2009 *Transmission Electron Microscopy: A Textbook for Materials Science* (Boston, MA: Springer US) pp. 53–71
[52] Zheng J C, Yang Z, He Z J, Tong H, Yu W J and Zhang J F 2018 *Nano Energy* **53** 613
[53] Wang Q, Shang M, Zhang Y, Yang Y and Wang Y 2018 *ACS Appl. Mater Interfaces* **10** 7162
[54] Gong Y, Chen Y, Zhang Q, Meng F, Shi J A, Liu X, Liu X, Zhang J, Wang H, Wang J, Yu Q, Zhang Z, Xu Q, Xiao R, Hu Y S, Gu L, Li H, Huang X and Chen L 2018 *Nat. Commun.* **9** 3341
[55] Li J, Hwang S, Guo F, Li S, Chen Z, Kou R, Sun K, Sun C J, Gan H, Yu A, Stach E A, Zhou H and Su D 2019 *Nat. Commun.* **10** 2224
[56] Lin F, Liu Y, Yu X, Cheng L, Singer A, Shpyrko O G, Xin H L, Tamura N, Tian C, Weng T C, Yang X Q, Meng Y S, Nordlund D, Yang W and Doeff M M 2017 *Chem. Rev.* **117** 13123
[57] Liang J, Li X, Zhao Y, Goncharova L V, Li W, Adair K R, Banis M N, Hu Y, Sham T K, Huang H, Zhang L, Zhao S, Lu S, Li R and Sun X 2019 *Advanced Energy Materials* **9** 1902125
[58] Li Y, Zhang W, Zheng Y, Chen J, Yu B, Chen Y and Liu M 2017 *Chem. Soc. Rev.* **46** 6345
[59] Wang L, Maxisch T and Ceder G 2007 *Chem. Materials* **19** 543
[60] Gao Y, Ma J, Wang X, Lu X, Bai Y, Wang Z and Chen L 2014 *J. Mater. Chem. A* **2** 4811
[61] Hoang K and Johannes M D 2012 *J. Power Sources* **206** 274
[62] Ouyang C Y, Shi S Q, Wang Z X, Li H, Huang X J and Chen L Q 2004 *J. Phys.: Condens. Matter* **16** 2265
[63] Yang J and Tse J S 2011 *J. Phys. Chem. A* **115** 13045
[64] Burkel E 2000 *Rep. Prog. Phys.* **63** 171
[65] Sette F, Krisch M H, Masciovecchio C, Ruocco G and Monaco G 1998 *Science* **280** 1550
[66] Price D L 1997 *Curr. Opin. Solid State Mater. Sci.* **2** 477
[67] Galeener F L, Leadbetter A J and Stringfellow M W 1983 *Phys. Rev. B* **27** 1052
[68] Baddour Hadjean R and Pereira Ramos J P 2010 *Chem. Rev.* **110** 1278
[69] Zhu W, Liu D, Trottier J, Gagnon C, Howe J, Mauger A, Julien C M and Zaghib K 2015 *J. Power Sources* **298** 341
[70] Senga R, Suenaga K, Barone P, Morishita S, Mauri F and Pichler T 2019 *Nature* **573** 247
[71] Yao Z, Kim S and He J 2018 *Sci. Adv.* **4** eaao6754
[72] Lepley N D, Holzwarth N A W and Du Y A 2013 *Phys. Rev. B* **88** 104103
[73] Shi S, Liu L, Ouyang C, Wang D S, Wang Z, Chen L and Huang X 2003 *Phys. Rev. B* **68** 195108
[74] Quartarone E and Mustarelli P 2011 *Chem. Soc. Rev.* **40** 2525
[75] He W, Wang D, Wu H, Xiao Y, Zhang Y, He D, Feng Y, Hao Y J, Dong J F, Chetty R, Hao L, Chen D, Qin J, Yang Q, Li X, Song J M, Zhu Y, Xu W, Niu C, Li X, Wang G, Liu C, Ohta M, Pennycook S J, He J, Li J F and Zhao L D 2019 *Science* **365** 1418
[76] Usachov D, Fedorov A, Vilkov O, Senkovskiy B, Adamchuk V K, Yashina L V, Volykhov A A, Farjam M, Verbitskiy N I, Gruneis A, Laubschat C and Vyalikh D V 2014 *Nano Lett.* **14** 4982
[77] Thomsen C and Reich S 2000 *Phys. Rev. Lett.* **85** 5214
[78] Martin R M and Falicov L M 1983 *Light Scattering in Solids I: Introductory Concepts* (Cardona M, Ed.) (Berlin, Heidelberg: Springer Berlin Heidelberg) pp. 79–145
[79] Zhang S, Zhang N, Zhao Y, Cheng T, Li X, Feng R, Xu H, Liu Z, Zhang J and Tong L 2018 *Chem. Soc. Rev.* **47** 3217
[80] Wu J B, Lin M L, Cong X, Liu H N and Tan P H 2018 *Chem. Soc. Rev.* **47** 1822
[81] Chen S Z, Deng Y X, Cao X H, Zhou W X, Feng Y X, Tang L M and Chen K Q 2019 *J. Mater. Chem. A* **7** 21976
[82] Seo D H, Lee J, Urban A, Malik R, Kang S and Ceder G 2016 *Nat. Chem.* **8** 692
[83] Milot R L and Schmuttenmaer C A 2015 *Acc Chem. Res.* **48** 1423
[84] Huang J Y, Zhong L, Wang C M, Sullivan J P, Xu W, Zhang L Q, Mao S X, Hudak N S, Liu X H, Subramanian A, Fan H Y, Qi L A, Kushima A and Li J 2010 *Science* **330** 1515
[85] Kim S, Yao Z, Lim J M, Hersam M C, Wolverton C, Dravid V P and He K 2018 *Adv. Mater* **30** e1804925
[86] Hu E, Wang X, Yu X and Yang X Q 2018 *Acc. Chem. Res.* **51** 290
[87] Zhou Y N, Yue J L, Hu E, Li H, Gu L, Nam K W, Bak S M, Yu X, Liu J, Bai J, Dooryhee E, Fu Z W and Yang X Q 2016 *Adv. Energy Mater.* **6** 1600597
[88] Leung K and Budzien J L 2010 *Phys. Chem. Chem. Phys.* **12** 6583
[89] Zhang T, Jiang Y, Song Z, Huang H, He Y, Fang Z, Weng H and Fang C 2019 *Nature* **566** 475